Int. J. Electrochem. Sci., 12 **(2017)** 6304 – 6314, doi: 10.20964/2017.07.60

International Journal of ELECTROCHEMICAL SCIENCE
www.electrochemsci.org

Label Free C-reactive Protein Detection Based on An Electrochemical Sensor for Clinical Application

Xuehua Bing[1,*], *Guorong Wang*[2]

[1] Department of Cardiovascular Surgery, the Central Hospital of Linyi, Shandong Province, 276400, Linyi, P. R. China
[2] Department of the Infection Control Section, the Central Hospital of Linyi, Shandong Province, 276400, Linyi, P. R. China
[*]E-mail: xuehuabing@foxmail.com

Received: 4 April 2017 / *Accepted:* 28 April 2017 / *Published:* 12 June 2017

This study describes the facile and effective fabrication of electrochemical biosensors based on a glassy carbon electrode coated with graphene quantum dots (GQD). The prepared electrode shows a desirable electrochemical response, since the graphene is favourably conductive. The prepared GQD designed biosensor has been employed for C-reactive protein (CRP) detection in blood serum. Herein, charge transfer resistance variations were significantly target specific, showing a linear relationship with log CRP concentration (0.5–70 nM) and a low limit of detection (LOD) of 176 pM. This technique could be employed to achieve one-step CRP detection and has the potential to be applied to clinical atrial fibrillation (AF) analysis after CABG.

Keywords: Atrial fibrillation; Electrochemical sensor; C-reactive protein; Graphene quantum dots; CABG

1. INTRODUCTION

It is vital for specific biomolecules to be rapidly, effectively and sensitively detected for the purposes of environmental protection, medical diagnosis and biological engineering [1]. A myriad of cost-effective, stable and sensitive biosensors have been developed from gold nanoparticles [2-4], carbon nanotubes [5-7], quantum dots [8-12] and many other nanomaterials. Recently, graphene has been proposed as an emerging nanomaterial due to its desirable features. This two-dimensional carbon material is measurable at a single atom thickness. Due to its favourable mechanical, electronic and thermal features and excellent chemical stability, it has attracted great attention for scientific studies [13-15]. Fluorescence studies have been performed that demonstrate the ability to selectively

and sensitively detect proteins and metal ions. Additionally, DNA has been detected using graphene oxide (GO) coupled with a dye-tagged single-stranded DNA (ssDNA) probe [16, 17]. Furthermore, graphene has been applied in electrode surface modification as a film material, contributing to significant improvement in electrochemical bio-sensing research [18-20].

A common complication of open heart surgery, atrial fibrillation/flutter (AF) is supposed to be prevented by ACC/AHA guideline-recommended prophylactic beta-blockers (BB). Despite several studies during the last few years, effective protection against AF by BB in patients undergoing post–coronary artery bypass graft surgery (CABG) has not been confirmed. Shifts in the demographic characteristics of the patients who have received open heart surgery and significant changes in the treatment of coronary artery disease (CAD) and the protocols of CABG have occurred in the last twelve years. The connection between high CRP levels and AF occurrence has been presumed. However, it is still uncertain whether high plasma CRP levels are only indicative of AF occurrence, or whether high CRP levels cause the disorder. These factors are clinically significant, since angiotensin receptor blockers, angiotensin-transforming enzyme inhibitors and several other cardiovascular drugs are applied to moderate the inflammation in heart [21, 22]. It is also significant because drugs that reduce CRP levels are prescribed for the treatment of cardiovascular-related disease [23]. Whether plasma CRP levels cause AF has been studied by means of Mendelian randomization [24], where genetic variants were randomly assorted with the production of gametes. The connection between high plasma CRP levels and AF occurrence was evaluated via the link between plasma CRP levels and particular genetic variants. Hence, genetic variants that are exclusively involved in high plasma CRP levels [25] could be employed to obtain lifetime CRP levels without the impedance of reverse causation [26].

This study used nanometre-sized graphene quantum dots (GQD) for a range of measurements. GQDs are superfine and shaped in a well-defined way. In addition to having the desirable features of its family members, GQD exhibit the favourable traits of a nanomaterial. Therefore, GQDs were employed herein to fabricate electrochemical biosensors. CRP determination in blood serum has been made through electrochemical analysis with GQDs. The GQD-based immunosensor could be used in AF analysis after CABG in the future.

2. EXPERIMENTS

2.1. Reagents

Bovine serum albumin (BSA), human blood serum, and human C-reactive protein (CRP) purchased from Sigma Aldrich. AbD Serotec was the material source for the goat anti-human CRP polyclonal antibody. N-hydroxysuccinimide (NHS), 1-ethyl-3-(3-dimethylaminopropyl) carbodiimide (EDC) and polyethylene glycol (PEG)-thiol HS-C_{11}-$(EG)_3$-OCH_2-COOH were purchased from Sigma Aldrich. Ultrapure water (18.2 MΩ/cm) from a Milli-Q system was employed for all the experiments. Phosphate buffered saline (PBS) tablets were purchased from Sigma Aldrich and dissolved in water

with Tween-20 (0.2% v/v) to synthesize PBST (10 mM, pH 7.4). Then, a membrane filter (0.22 μm) was employed to filter the obtained PBST. All other reagents were of analytical grade.

2.2. Synthesis of GQD

A modified Hummers technique was employed to transform the natural graphite powder into graphene oxide (GO) sheets [27, 28], which were then thermally reduced in a tube furnace for 120 min at 200–300 °C under nitrogen at a heating rate of 5 °C min^{-1} to synthesize graphene sheets (GSs). This was followed by the oxidization of 0.05 g GSs in concentrated solutions of 30 mL HNO_3 and 10 mL H_2SO_4 under mild ultrasonication (500 W, 40 kHz) for 15–20 h. Then, deionized water was used to dilute the mixed solution. Afterwards, a microporous membrane (0.22-μm) was utilized to filter the as-purified mixture for acids extraction. This was followed by a repeated dispersion of the obtained GSs (0.2 g) into 40 mL DI water. Through the addition of NaOH, the pH value of as-prepared dispersion was adjusted to 8. After being delivered into a poly(tetrafluoroethylene) (Teflon)-lined autoclave (50 mL), the obtained suspension was heated at 200 °C for 10 h, and cooled to ambient temperature. Subsequently, the microporous membrane (0.22-μm) was employed to filter the terminal black suspension to obtain a brown filter solution with a yield of approximately 22%. However, there remained several large graphene nanoparticles measured in a range of 50–200 nm in this colloidal solution, which resulted in the emission of weak blue fluorescence. Thus, further dialysis was performed on the terminal solution overnight in a dialysis bag with a retained molecular weight of 3500 Da. GQDs that were significantly fluorescent through the bag were obtained with a yield of approximately 5%.

2.3. Characterization

Cu K*α* radiation was applied to samples in a Rigaku D/max-2500 to conduct X-ray powder diffraction (XRD) measurements. A Hitachi 7000 fluorescence and a Hitachi 3100 spectrophotometer were employed to characterize fluorescence and absorption, respectively. A Renishaw in plus laser Raman spectrometer and a Bio-Rad FTIR spectrometer FTS165 were applied to Raman (λ_{exc} 785 nm) and FTIR measurements, respectively. A FRA2 module-equipped Autolab Potentiostat 12 (Metrohm Autolab B.V.) and a Kratos Axis Ultra DLD X-ray photoelectron spectrometer were employed to perform electrochemical and X-ray photoelectron spectroscopy (XPS) C 1s experiments, respectively. This work employed a traditional triple-electrode configuration, including a reference electrode, a counter electrode and a working electrode, taken by Ag/AgCl (CH Instruments), platinum wire and a gold disk (BASi) with a diameter of 1.6 mm.

2.4. Electrode fabrication

After being successively polished by 3.0, 1.0 and 0.1 μm diamond spray, the glassy carbon electrodes (GCE) were ultrasonically washed in water for approximately 5 min. Then, as-purified GCE

were immersed in freshly prepared piranha solution for 15 min and electrochemically polished via CV with a potential range of −0.1 and 1.25 V to obtain a stable reduction peak. Subsequently, nitrogen gas flow was conducted to dry the obtained GCE. This was followed by dropping GQD dispersion (5 μL) onto the surface of the electrode and drying at ambient temperature. Then, the as-prepared electrode was instantly immersed into a 10 mM solution of HS-C_{11}-$(EG)_3$-OCH_2-COOH in ethanol at ambient temperature for 16 h. After SAM was formed, the modified electrode was rinsed successively with ethanol and water. Then, nitrogen gas flow was applied to dry the electrode which was then incubated in a mixture of NHS (0.1 M) and EDC (0.4 M) for 15 min to activate terminal carboxyl groups. Then, the terminal electrode was fabricated after further incubation in 10 μM CRP antibody solution (PBST, pH 7.4) for 60 min prior to characterization.

2.5. Electrochemical impedance spectroscopy characterization

EIS was performed with a frequency range of 0.05 Hz to 10 kHz, the direct current potential of 0.25 V (1.0 mM $[Fe(CN)_6]^{3-/4-}$), and the amplitude of the applied potential sine wave was obtained at 10 mV. Nyquist plots (complicated plane profiles) were employed for EIS measurements in PBST solution (10 mM). In addition, an ideal Randles equivalent circuit was used for fitting the obtained data. The sensitivity of the EIS measurement was deduced from the slop of the Nyquist plot semi-cycles.

3. RESULTS AND DISCUSSION

Since diameters and widths as low as approximately 20 nm can be obtained via lithography methods, a majority of electronic apparatuses have been constructed with GQD and GNRs. Nevertheless, GQDs and GNRs have trouble with gaining smooth edges and require costly devices, which could be offset by other chemical approaches that also specialize in facile surface functionalization. Initially, ultrasmooth and functionalized GNRs with widths of 50 nm to sub-10 nm were realized via a chemical approach proposed by Li and co-workers [29]. Kosynkin and co-workers proposed a facile solution-based oxidative procedure not long ago, where the sidewalls of multiwall carbon nanotubes (CNT) were cut and unravelled longitudinally to synthesize GNRs [30]. However, the size of sub-10 nm functionalized GQDs has not been realized by any chemical approaches until now. This work proposes a facile and new hydrothermal method to obtain surface-functionalized GQDs with average diameters of approximately 9.6-nm by the cutting of GSs. Compared to GNRs and GSs with large lateral sizes, the as-prepared GQDs were observed to show bright blue photoluminescence (PL). The GQDs are superfine and exhibit a large edge effect, directly resulting in novel UV–vis absorption bands and blue luminescence. Originally, GO sheets were thermally reduced to obtain micrometre-sized rippled GSs. The obtained GSs were oxidized in concentrated solutions of HNO_3 and H_2SO_4 and then hydrothermally treated (Fig. 1A). There was a small decrease in GS size after they were oxidized, with a small increase in (002) spacing up to 3.85 Å. A series of more marked

changes occurred after the hydrothermal treatment of the oxidized GSs at 200 °C. First, the (002) spacing was reduced to 3.43 Å, very close to that of bulk graphite, indicating that deoxidization occurs during the hydrothermal process [31]. According to the Fourier transform infrared (FTIR) spectrum, C—O—C, OH, C=O/COOH and other oxygen-containing functional groups were found to be introduced on the basal plane and the edge during oxidization, as shown in Fig. 1B, where the solubility of the GSs in water was realized due to the appearance of the aforementioned groups. After hydrothermal treatment, the strongest vibrational absorption band of C=O/COOH at 1720 cm^{-1} became very weak and the vibration band of epoxy groups at 1052 cm^{-1} disappeared [32].

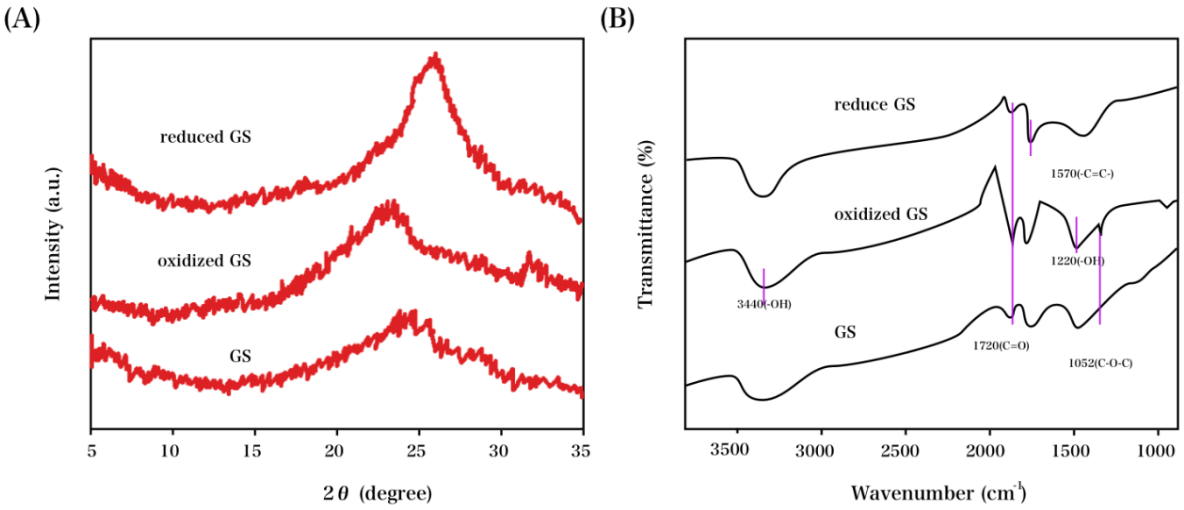

Figure 1. (A) XRD profiles and (B) FTIR spectra of the original, oxidized, and hydrothermally reduced GSs.

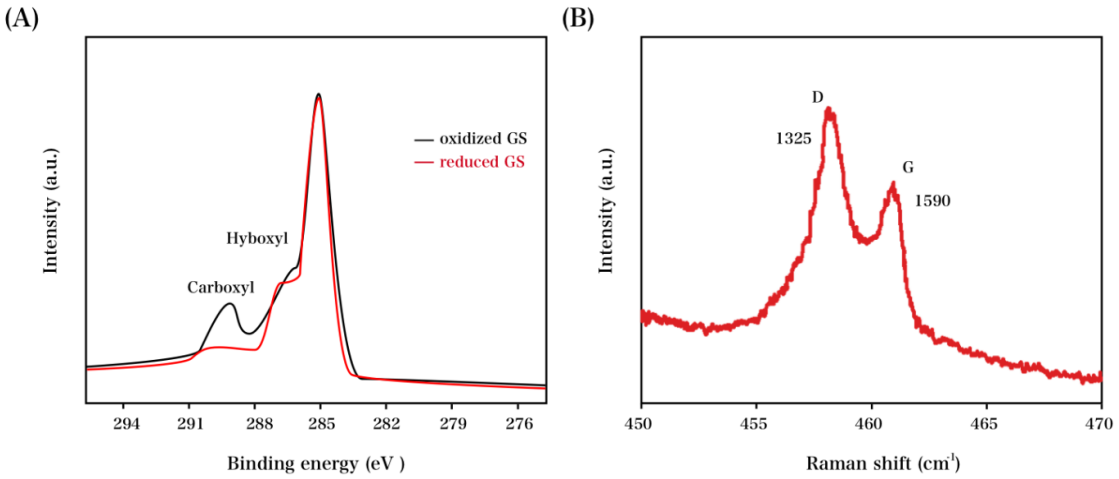

Figure 2. (A) XPS C_{1s} spectra of both oxidized and hydrothermally reduced GSs. (B) Raman spectrum of the hydrothermally reduced GSs.

The variations in XPS C1 s spectra provide further evidence for the reduction. The oxidized and hydrothermally reduced GSs were characterized via XPS C1 s spectra in Fig. 2A, and the reduced GSs were characterized via corresponding Raman spectrum in Fig. 2B. As indicated in the former

spectra, the signal at 288 eV indicates that there is a decrease in the strength of carboxyl groups after hydrothermal treatment, with an almost unvaried sp^2 carbon peak at 284.1 eV. The latter spectrum exhibits a D band and G band, respectively at 1324 cm^{-1} and 1588 cm^{-1}, with I_D/I_G (intensity ratio) calculated as 1.26.

As shown in Fig. 3A, the oxidized GSs and the GQDs dispersed in water were characterized via UV–vis absorption spectra, with pronounced variations. As indicated in the spectrum of the former one, a characteristic absorption peak was observed at approximately 230 nm, attributed to the π - π* transition of aromatic sp^2 regions. For the latter, a novel absorption band at approximately 320 nm could be monitored in addition to the strong π - π* absorption peak. The comparison between novel PL performances arouses the greatest interest. Even measured under alkali conditions, no detectable PL is exhibited for the oxidized GSs. For GQDs, bright blue luminescence is emitted even when measured in neutral conditions, as indicated in Fig. 3B. Fig. 3A exhibits a strong peak at 430 nm in the PL spectrum induced upon the excitation at the absorption band of 320 nm, with a Stokes shift of 110 nm at 0.99 eV. When measured with respect to a reference, the quinine sulphate, the PL quantum yield of GQDs is obtained as 7.2%, which is comparable with that obtained for the presented luminescent carbon nanoparticles. The PL performance of GQDs relies on excitation, which is similar to a majority of luminescent carbon nanoparticles. As indicated in Fig. 3B, there is a shift of the PL peak to longer wavelengths and a sharp reduction in the intensity when the excitation wavelength is increased from 320 to 420 nm. As shown in Fig. 3C, two significant peaks can be observed at 257 and 320 nm in the PL excitation spectrum, with the emission of the strongest luminescence. The PLE spectrum clearly demonstrates that the observed luminescence from the GQDs is directly correlated with the two new transitions at 257 and 320 nm rather than the commonly observed π–π* transition [33]. Both the 257-nm and 320-nm excitation results in the most significant PL peak at 430 nm. The absorption band observed at 320 nm is consistent with the PL excitation peak at 320 nm. An absorption band that can hide in the strong background absorption from the π–π* transition ought to correspond with the PL excitation peak at 257 nm. Instead of the ordinary π–π* transition, novel transitions observed at 257 and 320 nm are in direct correlation with the GQDs-emitted luminescence, as indicated previously in the PL excitation spectrum.

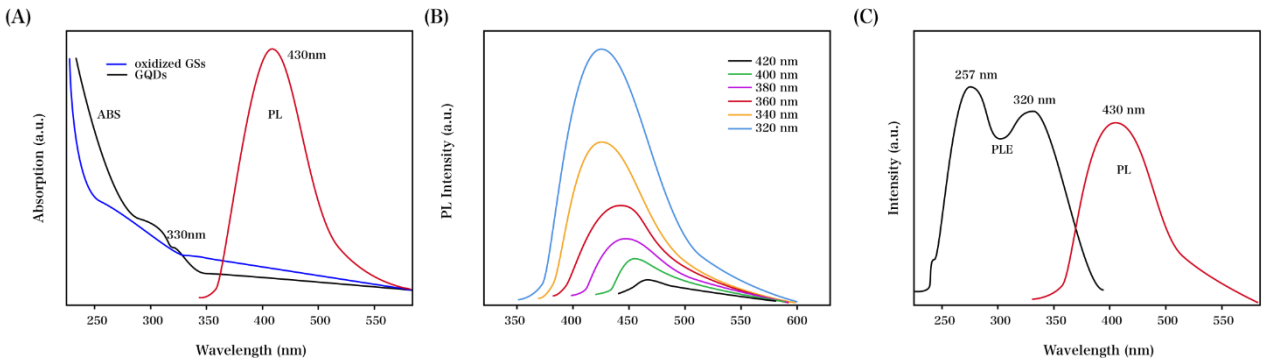

Figure 3. (A) UV–vis absorption and PL spectra of the GQDs dispersed in water. (B) PL spectra of the GQDs at varied excitation wavelengths. (C) PLE spectrum with the detection wavelength of 430 nm and PL spectrum excited at 257 nm.

The step-by-step construction of a receptive surface can be well characterized via an EIS measurement. The electrostatically or sterically imposed charge transportation restrictions with the fabrication of the films are presented by the semicircles at low frequency in Nyquist plots. With the construction of the receptor layer, R_{ct} increases significantly as expected. After the successful formation of PEG SAM, there is a rather distinct increase in R_{ct} (less than 4 kΩ/cm^2 to ~45 MΩ/cm^2), which further increases upon the immobilization of the antibody, as indicated in Fig. 4. Herein, as the antibody is successfully immobilized, the interfacial steric bulk increases, corresponding to the dramatic R_{ct} increase. This is followed by a consistent response of interface resistance to the binding of target protein that can be used for calibration.

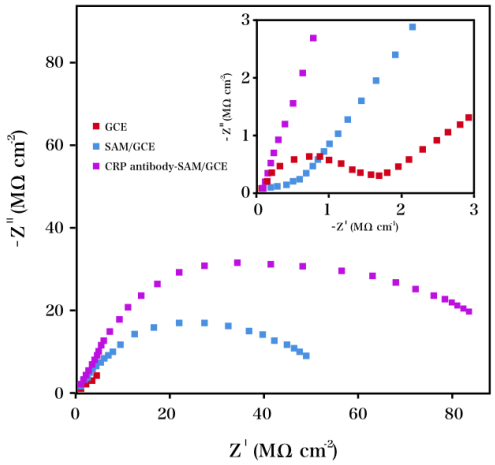

Figure 4. Nyquist plots of GCE, SAM/GCE and CRP antibody-SAM/GCE recorded in PBST (10 mM, pH 7.4) solution containing 1.0 mM $[Fe(CN)_6]^{3-/4-}$. The inset highlights the high frequency domain.

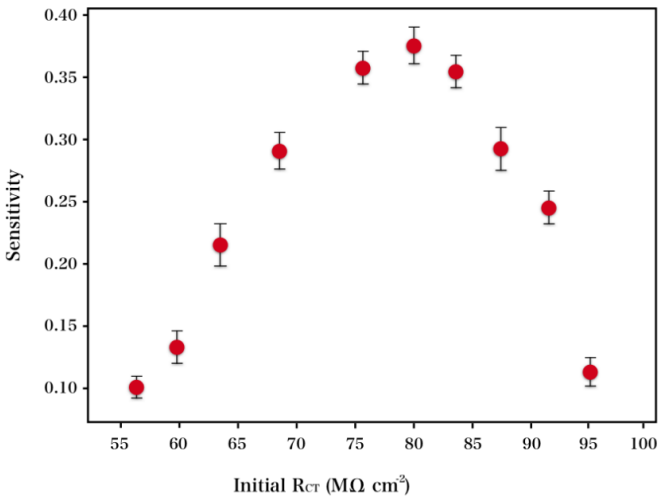

Figure 5. Relationship between initial *Rct* and the sensitivity of the GQD-based CRP biosensor. The slope exhibited in the calibration curve of the sensor was for the characterization of the sensitivity. The CRP concentrations for these tests ranged from 0.5 to 50 nM.

It has been presumed that the initial resistance has an effect on the sensitivity detected afterwards. To be specific, if there is a relatively low resistance for the receptor layer initially, more dramatic increases and more significant measurement sensitivity would naturally be expected, considering the increase in charge transportation resistance is the base for the measurement. The density of antibody surface is a factor in changing the aforementioned initial resistance, where the adjustment of incubation concentration or time could control it during the fabrication of the layer. The sensitivity of the measurement shows a correlation with the initial layer charge transportation resistance, as shown in Fig. 5. Note that there is an increase in measurement sensitivity by more than 400% with a reduction of the antibody surface coverage. Then, a decrease is expected with decreases in the density of functional surface-bound antibodies, lower than the level for efficacious specific target binding. These observations are robust and reproducible across numerous assays. We believe them to be general and, from a practical perspective, to have considerable value in the construction of optimally responsive interfaces [34].

CRP screening was performed in PBST at the proposed interfaces. A dissociation constant K_D can be derived as 1.1±0.11 nM, according to a gradual increase in (and ultimately saturation of) *Rct* with concentration, as indicated in Fig. 6. There is a linear increase in *Rct* with logarithmic sensitivity of CRP concentration (0.5–60 nM) before saturation, with a detection limit as low as 140 pM, which indicates a desirable sensitivity for real sample detection. The prepared interfaces are, additionally, unresponsive (<3% change in signal) to BSA levels of up to 100 nM, an observation we ascribe to the excellent antifouling properties [35].

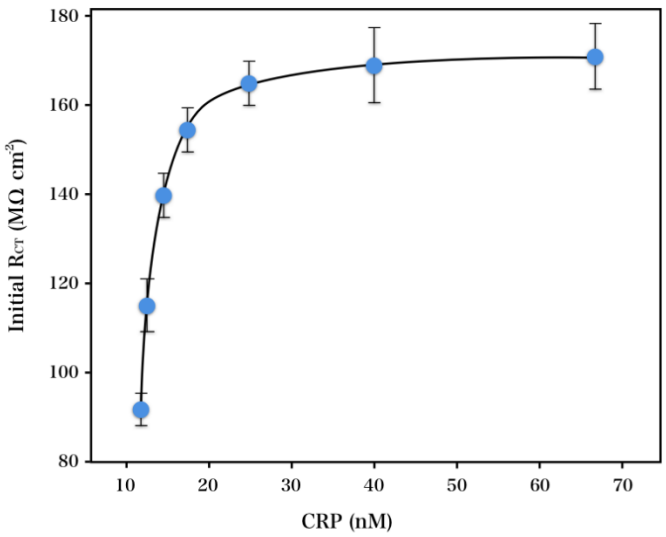

Figure 6. Recorded charge-transfer resistance (*Rct*) of the GQD-based CRP biosensor after being incubated with varied concentrations of CRP protein (from 10 to 70 nM) in PBST (10 mM, pH 7.4) containing 1.0 mM $[Fe(CN)_6]^{3-/4-}$.

It is essential for CRP to be conveniently and directly detected in blood serum for clinical application, which is extremely tough in nearly all tag-free detection. However, with a desirable master of the electrode interfaces and the low response obtained to high BSA levels demonstrated in the

system above, we proposed two approaches to CRP screening in blood serum. In terms of the former capacity, the controllable dilution in PBST allows for the *in situ* detection of CRP spiked blood serum, as indicated in Fig. 7. Herein the linear detection was reliable within a clinically relevant range with a low detection limit of 170 pM. To allow realistic comparison with previous reports, the characteristics of different electrochemical sensors for clenbuterol are summarized in Table 1.

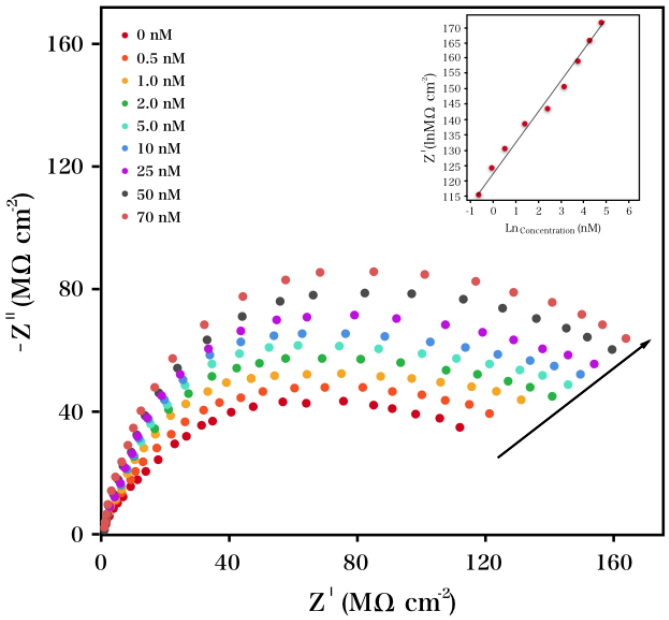

Figure 7. Faradaic impedance spectra corresponding to the biosensor after the incubation in PBST solution containing human blood serum (10%) and $Fe(CN)_6^{3-/4-}$ (1.0 mM), with varied CRP concentrations: 0, 0.5, 1.0, 2.0, 5.0, 10, 25, 50 and 70 nM.

Table 1. Comparison of the major characteristics of electrochemical sensors used in the determination of CRP protein.

Electrode	Linear detection range	Detection limit	Reference
ZnO nanotubes	2-60 nM	0.7 nM	[36]
Carbon nanofiber	5-40 nM	2.1 nM	[37]
Chemiluminescence determination	1-100 nM	0.4 nM	[38]
GQD-based CRP biosensor	0.5–70 nM	170 pM	This work

As shown in Table 2, the data for the six sera of blood specimens obtained from ELISA and the GQD technique were compared, together with their relative deviations, to study the accuracy of CRP detection. The relative error was in the range of 1.9% to 8.1%. Thus, it could be concluded that the two methods were desirably coherent with each other. Hence, the requirements of a CRP electrochemical sensor could be well met by the designed technique to serve for clinical AF analysis after CABG.

Table 2. Experimental results comparison of varied analytical techniques obtained for blood specimens.

Blood samples	1	2	3	4	5	6
Proposed sensor in this work (nM)	1.05	5.04	10.03	24.43	51.20	72.6
ELISA (ng/ml)	1.14	5.13	9.96	23.41	50.36	74.3
Relative deviation (%)	5.6	7.8	3.5	5.5	1.9	8.1

4. CONCLUSIONS

This work addressed the fabrication of an electrochemical biosensor based on GQD-modified GCE to achieve selective and sensitive CRP detection. Due to the stability and favourably low detection limit, this biosensor has the potential to be applied to clinical AF analysis after CABG.

References

1. J. Wang, *Anal. Chim. Acta.*, 500 (2003) 247.
2. S. Park, T. Taton and C. Mirkin, *Science*, 295 (2002) 1503.
3. H. Li and L. Rothberg, *Proceedings of the National Academy of Sciences of the United States of America*, 101 (2004) 14036.
4. M. Rueping, A. Antonchick and T. Theissmann, *Angewandte Chemie International Edition*, 45 (2006) 3683.
5. X. Yu, D. Chattopadhyay, I. Galeska, F. Papadimitrakopoulos and J. Rusling, *Electrochemistry Communications*, 5 (2003) 408.
6. J. Ye, Y. Wen, W. De Zhang, L. Gan, G. Xu and F. Sheu, *Electrochemistry Communications*, 6 (2004) 66.
7. X. Zhang, K. Jiao, S. Liu and Y. Hu, *Anal. Chem.*, 81 (2009) 6006.
8. J. Wang, G. Liu, M. Jan and Q. Zhu, *Electrochemistry Communications*, 5 (2003) 1000.
9. S. Dwarakanath, J.G. Bruno, A. Shastry, T. Phillips, A. John, A. Kumar and L.D. Stephenson, *Biochemical and biophysical research communications*, 325 (2004) 739.
10. L. Shi, V. De Paoli, N. Rosenzweig and Z. Rosenzweig, *Journal of the American Chemical Society*, 128 (2006) 10378.
11. J. Choi, K. Chen and M. Strano, *Journal of the American Chemical Society*, 128 (2006) 15584.
12. S. Gac, I. Vermes and A. Berg, *Nano Letters*, 6 (2006) 1863.
13. M. Daly, E. Gaidamakova, V. Matrosova, A. Vasilenko, M. Zhai, A. Venkateswaran, M. Hess, M. Omelchenko, H. Kostandarithes and K. Makarova, *Science*, 306 (2004) 1025.
14. A. Ferrari, J. Meyer, V. Scardaci, C. Casiraghi, M. Lazzeri, F. Mauri, S. Piscanec, D. Jiang, K. Novoselov and S. Roth, *Physical Review Letters*, 97 (2006) 187401.
15. A. Geim, *Science*, 324 (2009) 1530.
16. C. Lu, H. Yang, C. Zhu, X. Chen and G. Chen, *Angewandte Chemie*, 121 (2009) 4879.
17. S. He, B. Song, D. Li, C. Zhu, W. Qi, Y. Wen, L. Wang, S. Song, H. Fang and C. Fan, *Adv Funct Mater*, 20 (2010) 453.
18. M. Zhou, Y. Zhai and S. Dong, *Anal. Chem.*, 81 (2009) 5603.
19. Y. Huang, X. Dong, Y. Shi, C. Li, L. Li and P. Chen, *Nanoscale*, 2 (2010) 1485.
20. S. Alwarappan, A. Erdem, C. Liu and C. Li, *J Phys Chem C*, 113 (2009) 8853.
21. O. Pedersen, H. Bagger, L. Køber and C. Torp-Pedersen, *Circulation*, 100 (1999) 376.
22. K. Wachtell, M. Lehto, E. Gerdts, M. Olsen, B. Hornestam, B. Dahlöf, H. Ibsen, S. Julius, S. Kjeldsen and L. Lindholm, *Journal of the American College of Cardiology*, 45 (2005) 712.

23. G. Lowe and M. Pepys, *Current atherosclerosis reports*, 8 (2006) 421.
24. G. Smith and S. Ebrahim, *International journal of epidemiology*, 33 (2004) 30.
25. C. Carlson, S. Aldred, P. Lee, R. Tracy, S. Schwartz, M. Rieder, K. Liu, O. Williams, C. Iribarren and E.. Lewis, *The American Journal of Human Genetics*, 77 (2005) 64.
26. J. Zacho, A. Tybjærg-Hansen, J. Jensen, P. Grande, H. Sillesen and B. Nordestgaard, *N. Engl. J. Med.*, 359 (2008) 1897.
27. Y. Xu, H. Bai, G. Lu, C. Li and G. Shi, *Journal of the American Chemical Society*, 130 (2008) 5856.
28. D. Pan, J. Zhang, Z. Li and M. Wu, *Adv. Mater.*, 22 (2010) 734.
29. X. Li, X. Wang, L. Zhang, S. Lee and H. Dai, *Science*, 319 (2008) 1229.
30. D. Kosynkin, A. Higginbotham, A. Sinitskii, J. Lomeda, A. Dimiev, B. Price and J.. Tour, *Nature*, 458 (2009) 872.
31. L. Stobinski, B. Lesiak, A. Malolepszy, M. Mazurkiewicz, B. Mierzwa, J. Zemek, P. Jiricek and I. Bieloshapka, *Journal of Electron Spectroscopy and Related Phenomena*, 195 (2014) 145.
32. W. Lin, H. Chang and R. Wu, *Sensors and Actuators B: Chemical*, 181 (2013) 326.
33. M. Li, W. Wu, W. Ren, H. Cheng, N. Tang, W. Zhong and Y. Du, *Applied Physics Letters*, 101 (2012) 103107.
34. T. Bryan, X. Luo, P. Bueno and J. Davis, *Biosensors and Bioelectronics*, 39 (2013) 94.
35. N. Alcantar, E. Aydil and J. Israelachvili, *Journal of Biomedical Materials Research*, 51 (2000) 343.
36. Z. Ibupoto, N. Jamal, K. Khun and M. Willander, *Sensors and Actuators B: Chemical*, 166 (2012) 809.
37. R. Gupta, A. Periyakaruppan, M. Meyyappan and J. Koehne, *Biosensors and Bioelectronics*, 59 (2014) 112.
38. S. Wang, E. Harris, J. Shi, A. Chen, S. Parajuli, X. Jing and W. Miao, *Phys Chem Chem Phys*, 12 (2010) 10073.